INTERNATIONAL JOURNAL OF
NUMERICAL ANALYSIS AND MODELING
Volume 6, Number 3, Pages 375–388

WELL FLOW MODELS FOR VARIOUS NUMERICAL METHODS

ZHANGXIN CHEN AND YOUQIAN ZHANG

This paper is dedicated to the special occasion of Professor Roland Glowinski's 70th birthdate.

Abstract. Numerical simulation of fluid flow and transport processes in the subsurface must account for the presence of wells. The pressure at a gridblock that contains a well is different from the average pressure in that block and different from the flowing bottom hole pressure for the well [17]. Various finite difference well models have been developed to account for the difference. This paper presents a systematical derivation of well models for other numerical methods such as standard finite element, control volume finite element, and mixed finite element methods. Numerical results for a simple well example illustrating local grid refinement effects are given to validate these well models. The well models have particular applications to groundwater hydrology and petroleum reservoirs.

Key words. Well models, petroleum reservoirs, aquifer remediation, finite difference, finite element, control volume finite element, mixed finite element, fluid flow, numerical experiments

1. Introduction

Numerical simulation of fluid flow and transport processes in the subsurface must account for the presence of wells. The pressure at a gridblock that contains a well is different from the average pressure in that block and different from the flowing bottom hole pressure for the well [17]. The difficulty in modeling wells in a field scale numerical simulation is that the region where pressure gradients are the largest is closest to a well and is far smaller than the spatial size of gridblocks. Using local grid refinement around the well can alleviate this problem but can lead to an impratical restriction on time step sizes in the numerical simulation [5]. The fundamental task in modeling wells is to model flows into the wellbore accurately and to develop accurate well equations that allow the computation of the bottom hole pressure when a production or injection rate is given, or the computation of the rate when this pressure is known.

The first theoretical study of well equations was given by Peaceman [17] for cell-centered finite difference methods on square grids for single phase flow. Peaceman's study gave a proper interpretation of a well-block pressure, and indicated how it relates to the flowing bottom hole pressure. The importance of his study is that the computed block pressure is associated with the steady-sate pressure for the actual well at an equivalent radius r_e. For a square grid with a grid size h, Peaceman derived a formula for r_e by three different approaches: (1) analytically by assuming that the pressure in the blocks adjacent to the well block is computed exactly by the radial flow model, obtaining $r_e = 0.208h$, (2) numerically by solving the pressure equation on a sequence of grids, deriving $r_e = 0.2h$, and (3) by solving exactly the system of difference equations and using the equation for the pressure drop between the injector and producer in a repeated five-spot pattern problem, finding $r_e = 0.1987h$. From these approaches, he concluded that $r_e \approx 0.2h$.

Received by the editors August 30, 2008.
2000 *Mathematics Subject Classification.* 65N30, 65N10, 76S05, 76T05.

Peaceman's finite difference well models on square grids have been extended in various directions, including to rectangular grids, anisotropic reservoirs, horizontal wells, and multiphase flows and to incorporating gravity force, skin, and non-Darcy effects. Peaceman himself extended his classical well model [17] to more general scenarios [18] where rectangular grids and anisotropic permeabilities are allowed. For the treatment of arbitrary well locations and horizontal wells, the reader can refer to [2, 19]. Lee and Milliken [13] studied an arbitrary monobore well in a layered system of laterally infinite extent. They combined a semianalytical solution based on slender body theory with a finite difference pressure solution with lateral pressure boundary conditions described by the semianalytical solution. Ding [8] introduced a layer potential function to obtain a steady state pressure distribution in the vicinity of the well. Furthermore, he adjusted well block transmissibilities to account for radial flow. Later, Ding and Jeannin [9] developed a multipoint discretization in a curvilinear coordinate system and used the discretization coefficient of an elliptic equation as the well index. Recently, Wolfsteiner et al. [22] extended Peaceman's well models to account for different well configurations in heterogeneous porous media. More recently, Chen and Yue [6] derived a well model by introducing multiscale basis functions that resolve well singularity, and Aarnes [1] proposed a modified mixed multiscale finite element method that can account for radial flow near a well. Finally, Ewing et al. [10] and Garanzha et al. [11] developed numerical well models that account for non-Darcy effects.

As far as the authors know, however, most of these existing well models have been developed for finite difference methods [8, 17, 19]. On the other hand, finite element methods have been successfully applied for numerical simulation of fluid flow and transport processes in the subsurface due to their intrinsic grid flexibility [5]. Thus it is clear that, to use finite element approximations in the presence of wells, accurate well models must be derived for this important class of numerical methods.

This paper presents a systematical derivation of well models for finite element approximations of three types: (1) standard finite element methods, (2) control volume finite element methods, and (3) mixed finite element methods. Extensions of these numerical well models to anisotropic reservoirs, horizontal wells, and multiphase flows and to incorporating gravity forces and skin factors are also discussed. For uniform grids and isotropic reservoirs, Peaceman's second approach for deriving well models will be used. When the grids are nonuniform or the reservoirs are anisotropic, we will make remarks on Peaceman's third approach. Numerical results for a simple well example illustrating local grid refinement effects are given to validate the well models derived. To motivate the derivation of finite element well models, the derivation of finite difference models is briefly reviewed.

The rest of the paper is organized as follows. The development of well equations requires the use of analytical formulas, which is given in the second section. In the third section, finite difference models are reviewed. The derivation of well models for the standard, control volume, and mixed finite element methods is carried out, respectively, in the fourth, fifth, and sixth sections. The seventh section is devoted to numerical results. The well model equations derived in this paper have particular applications to numerical simulation of aquifer remediation and of enhanced oil recovery, for example.

2. Analytical Formulas

The derivation of well flow equations is based on a basic assumption that the flow is radial in a neighborhood of the well, and requires the use of analytical formulas for radial flow. These formulas are known only in simplified flow situations. Thus we consider single phase incompressible flow in isotropic reservoirs. Furthermore, we focus on steady state flow. In the steady state case, the mass conservation equation is [3, 5]

$$\nabla \cdot (\rho \mathbf{u}) = q\delta, \tag{2.1}$$

where ρ and $\mathbf{u}$ are the density and volumetric velocity of the fluid, respectively, δ is the Dirac delta function representing a well placed at the origin, for example, and q is the mass production/injection at this well. Darcy's law without the gravity term is

$$\mathbf{u} = -\frac{1}{\mu}\mathbf{k}\nabla p, \tag{2.2}$$

where $\mathbf{k}$ is the absolute permeability tensor of the reservoir and p and μ are the fluid pressure and viscosity, respectively.

To obtain an analytical solution for equations (2.1) and (2.2), we assume that:

- The flow is two dimensional in x_1 and x_2 (i.e., it is homogeneous in the x_3-direction).
- The reservoir is homogeneous and isotropic; i.e., $\mathbf{k} = k\mathbf{I}$ and k is a constant.
- The viscosity μ and density ρ are constant.
- The flow is radial in a small neighborhood of the well.

With the last assumption, near the well the velocity $\mathbf{u}$ has the form

$$\mathbf{u}(r,\theta) = u(r)(\cos\theta, \sin\theta),$$

where (r,θ) is the polar coordinate system. Since the well is placed at the origin, substitution of this velocity into equation (2.1) gives

$$\frac{du}{dr} + \frac{1}{r}u = 0, \qquad r > 0, \tag{2.3}$$

whose solution is $u = C/r$. The constant C is proportional to q. Note that q represents the mass production/injection. Hence, when the well is an injector, for example, for any small neighborhood B of the origin (a small circle) q is the mass flux

$$q = h_3 \int_B \rho\mathbf{u}\cdot\boldsymbol{\nu}\, da(\mathbf{x}) = 2\pi\rho h_3 C; \quad \text{i.e.,} \quad C = \frac{q}{2\pi\rho h_3},$$

where $\boldsymbol{\nu}$ is the outward unit normal to B and h_3 is the reservoir thickness (or the height of the gridblock containing the well). Consequently, we obtain

$$\mathbf{u} = \frac{q}{2\pi\rho h_3 r}(\cos\theta, \sin\theta). \tag{2.4}$$

Substituting (2.4) into (2.2), taking a dot product of the resulting equation with $\boldsymbol{\nu} = (1,0)$, and integrating from $(r^o,0)$ to $(r,0)$, we obtain

$$p(r) = p(r^o) - \frac{\mu q}{2\pi\rho k h_3}\ln\left(\frac{r}{r^o}\right), \tag{2.5}$$

where $(r^o,0)$ is a reference point (e.g., r^o is the well radius r_w). Equation (2.5) is the analytical flow model near the well, on which the development of well equations for various numerical methods is based in the next four sections.

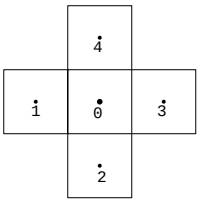

Fig. 3.1. Cell-centered difference on a square grid.

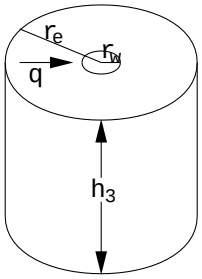

Fig. 3.2. Radial flow.

3. Finite Difference Methods

3.1. Square grids. For a square grid K_h, we solve equations (2.1) and (2.2) in the case where the well is located in the center of a grid cell. The adjacent cells are enumerated as in Fig. 3.1. Application of a five-point stencil scheme to (2.1) and (2.2) gives

$$\frac{\rho k h_3}{\mu}\left(4p_0 - p_1 - p_2 - p_3 - p_4\right) = q. \tag{3.1}$$

Using the symmetry of the solution p, i.e., $p_1 = p_2 = p_3 = p_4$, we see that

$$\frac{\rho k h_3}{\mu}\left(p_0 - p_1\right) = \frac{q}{4}. \tag{3.2}$$

We assume that the pressure at the adjacent cells is computed accurately. In particular, this means that the analytical well model derived in the previous section can be an accurate approximation in cell 1. Thus, if a bottom hole pressure p_{bh} is given, then it follows from equation (2.5) that

$$p_1 = p_{bh} - \frac{\mu q}{2\pi\rho k h_3}\ln\left(\frac{r_1}{r_w}\right), \tag{3.3}$$

where we recall that r_w is the well radius and $r_1 = h$. Inserting equation (3.3) into (3.2) yields

$$\begin{aligned} p_0 &= p_{bh} - \frac{\mu q}{2\pi\rho k h_3}\ln\left(\frac{h}{r_w}\right) + \frac{q\mu}{4\rho k} \\ &= p_{bh} + \frac{\mu q}{2\pi\rho k h_3}\left(\ln\left(\frac{r_w}{h}\right) + \frac{\pi}{2}\right) \\ &= p_{bh} + \frac{\mu q}{2\pi\rho k h_3}\ln\left(\frac{r_w}{\alpha_1 h}\right), \end{aligned}$$

where $\alpha_1 = e^{-\pi/2} = 0.20788\ldots$. This is exactly Peaceman's well model:

$$q = \frac{2\pi\rho k h_3}{\mu\ln(r_e/r_w)}(p_{bh} - p), \tag{3.4}$$

where the equivalent radius equals $r_e = \alpha_1 h = 0.20788h$ and $p = p_0$ (Fig. 3.2). The equivalent radius is the radius at which the steady state flowing pressure for the actual well equals the numerically computed pressure for the well cell. When the well is a producer, q is

$$q = \frac{2\pi\rho k h_3}{\mu\ln(r_e/r_w)}(p - p_{bh}). \tag{3.5}$$

3.2. Extensions.

3.2.1. Extension to anisotropic media. The well model (3.4) (or (3.5)) needs be extended in various directions, including to rectangular grids, anisotropic reservoirs, horizontal wells, and multiphase flows and to incorporating gravity force and skin effects. The gravitational effects must be treated on the same footing as pressure gradient effects. The skin factor s_k is a dimensionless number, and accounts for the effect resulting from formation damage caused by drilling. With these effects for single phase flow for an anisotropic permeability $\mathbf{k} = \mathrm{diag}(k_{11}, k_{22}, k_{33})$, the well model is extended to

$$q = \frac{2\pi\rho h_3\sqrt{k_{11}k_{22}}}{\mu\left(\ln(r_e/r_w) + s_k\right)}\left(p_{bh} - p - \rho\wp(z_{bh} - z)\right), \tag{3.6}$$

where $\wp$ is the magnitude of the gravitational acceleration, z is the depth, and z_{bh} is the well datum level depth. The factor $\sqrt{k_{11}k_{22}}$ comes from the coordinate transformation: $x_1' = x_1/\sqrt{k_{11}}$ and $x_2' = x_2/\sqrt{k_{22}}$ [5].

In the non-square grid and anisotropic medium case, the equivalent radius r_e can be calculated using Peaceman's third approach [18]

$$r_e = \frac{0.14\left(\left(k_{22}/k_{11}\right)^{1/2}h_1^2 + \left(k_{11}/k_{22}\right)^{1/2}h_2^2\right)^{1/2}}{0.5\left(\left(k_{22}/k_{11}\right)^{1/4} + \left(k_{11}/k_{22}\right)^{1/4}\right)}, \tag{3.7}$$

where h_1 and h_2 are the x_1- and x_2-grid sizes of the gridblock that contains the vertical well. The well index is defined by

$$WI = \frac{2\pi h_3\sqrt{k_{11}k_{22}}}{\ln(r_e/r_w) + s_k}. \tag{3.8}$$

3.2.2. Extension to horizontal wells. Horizontal wells in either the x_1- or the x_2-coordinate direction use the same well model equations as vertical ones. Only the parameters related to the direction of the wellbore need be modified. The well index for a horizontal well parallel to the x_1-direction is calculated:

$$WI = \frac{2\pi h_1\sqrt{k_{22}k_{33}}}{\ln(r_e/r_w) + s_k}; \tag{3.9}$$

if the well is parallel to the x_2-direction, it is

$$WI = \frac{2\pi h_2\sqrt{k_{11}k_{33}}}{\ln(r_e/r_w) + s_k}. \tag{3.10}$$

Accordingly, in the x_1-direction the equivalent radius r_e is

$$r_e = \frac{0.14\left(\left(k_{33}/k_{22}\right)^{1/2}h_2^2 + \left(k_{22}/k_{33}\right)^{1/2}h_3^2\right)^{1/2}}{0.5\left(\left(k_{33}/k_{22}\right)^{1/4} + \left(k_{22}/k_{33}\right)^{1/4}\right)}, \tag{3.11}$$

and in the x_2-direction,

$$r_e = \frac{0.14\left(\left(k_{33}/k_{11}\right)^{1/2}h_1^2 + \left(k_{11}/k_{33}\right)^{1/2}h_3^2\right)^{1/2}}{0.5\left(\left(k_{33}/k_{11}\right)^{1/4} + \left(k_{11}/k_{33}\right)^{1/4}\right)}. \tag{3.12}$$

A well in an arbitrary direction (i.e., a slanted well) cannot be easily modeled via finite difference methods. It will be discussed in the fifth section.

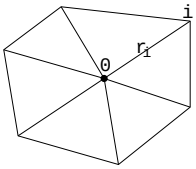

Fig. 4.1. Support Ω_0 of φ_0.

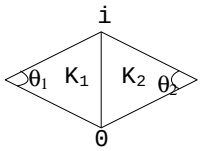

Fig. 4.2. Two adjacent triangles.

3.2.3. Extension to multiphase flow. The vertical well equations derived for single phase flow can be extended to multiphase flow, e.g., to a flow system of water, oil, and gas:

$$q_\alpha = \frac{2\pi h_3\sqrt{k_{11}k_{22}}}{\ln(r_e/r_w)+s_k}\frac{\rho_\alpha k_{r\alpha}}{\mu_\alpha}\left(p_{bh}-p_\alpha-\rho_\alpha g(z_{bh}-z)\right), \tag{3.13}$$

where ρ_α, $k_{r\alpha}$, and p_α are the density, relative permeability, and pressure of phase α, respectively, $\alpha = w, o, g$. Note that the definitions of the well index WI and equivalent radius r_e remain the same. A similar extension to horizontal wells for multiphase flow can be carried out as in Section 3.2.2.

4. Standard Finite Element Methods

The well equations derived in the context of finite differences can be extended to finite elements. For finite difference methods, the pressure at the well cell is numerically computed, and the pressure at the adjacent cells is computed using the analytical formula (2.5). This approach is also employed in the context of finite elements. Again, we concentrate on two-dimensional flow. Finite element methods have already been successfully applied for numerical simulation of fluid flow and transport processes in the subsurface due to their intrinsic grid flexibility [5]. Thus it is necessary to develop well equations for this important class of methods.

4.1. Triangular finite elements. For simplicity, we consider the case where the finite element space V_h is the space of piecewise linear polynomials associated with a triangulation K_h [4, 7]. As an illustration that the present derivation also applies to an anisotropic medium, we consider the anisotropic case in detail for the triangular elements. Extensions from the isotropic to anisotropic cases for other finite elements can be similarly carried out.

Let $\varphi_0 \in V_h$ be the basis function at node $\mathbf{x}_0$ where the well is located, and Ω_0 be the support of φ_0 (Fig. 4.1). Then, using equations (2.1) and (2.2), we see that

$$\frac{\rho h_3}{\mu}\sum_{K\subset\Omega_0}\int_K \mathbf{k}\nabla p\cdot\nabla\varphi_0\, d\mathbf{x} = q, \tag{4.1}$$

where the K's are the triangles in Ω_0. Let φ_i be the basis function at node $\mathbf{x}_i$ adjacent to node $\mathbf{x}_0$. Since $p = \sum_i \varphi_i p_i$ on Ω_0, it follows from (4.1) that

$$\frac{\rho h_3}{\mu}\sum_{K\subset\Omega_0}\sum_i\left(\int_K(\mathbf{k}\nabla\varphi_i)\cdot\nabla\varphi_0\, d\mathbf{x}\right)p_i = q. \tag{4.2}$$

Applying the properties of basis functions [4], this equation can be written:

$$-\frac{\rho h_3}{\mu}\sum_i T_{0i}(p_i-p_0) = q, \tag{4.3}$$

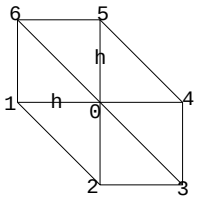

Fig. 4.3. Example of K_h near the well.

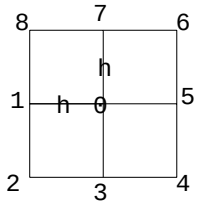

Fig. 4.4. Support Ω_0 for the bilinears.

where the transmissibility coefficient T_{0i} between nodes $\mathbf{x}_i$ and $\mathbf{x}_0$ is (Fig. 4.2)

$$T_{0i} = -\sum_{l=1}^{2} \left(|K_l| \left(\mathbf{k} \nabla \varphi_i \right) \cdot \nabla \varphi_0 \right) \Big|_{K_l}, \tag{4.4}$$

with $|K_l|$ the area of K_l (Fig. 4.2). System (4.3) is the linear system of algebraic equations arising from the finite element discretization of equations (2.1) and (2.2) at node $\mathbf{x}_0$.

We consider a homogeneous anisotropic medium in the vicinity of the well: $\mathbf{k} = \operatorname{diag}(k_{11}, k_{22}, k_{33})$ (i.e., k_{11}, k_{22}, and k_{33} are positive constants). Using the coordinate transform

$$x_1' = \frac{x_1}{\sqrt{k_{11}}}, \quad x_2' = \frac{x_2}{\sqrt{k_{22}}},$$

the transmissibility coefficient T_{0i} becomes

$$T_{0i} = \sqrt{k_{11} k_{22}} \left(\frac{\cot \theta_{K_1'} + \cot \theta_{K_2'}}{2} \right), \tag{4.5}$$

where $\theta_{K_1'}$ and $\theta_{K_2'}$ are the opposite angles of the two triangles in the transformed plane.

At an adjacent node $\mathbf{x}_i$, the analytic model in (2.5) is used to find the pressure

$$p_i = p_{bh} - \frac{\mu q}{2\pi\rho\sqrt{k_{11}k_{22}}h_3} \ln\left(\frac{r_i}{r_w}\right), \tag{4.6}$$

where r_i is the distance between $\mathbf{x}_i$ and $\mathbf{x}_0$. Substituting (4.6) into (4.3) gives the well model equation

$$q = \frac{2\pi\rho\sqrt{k_{11}k_{22}}h_3}{\mu \ln(r_e/r_w)}(p_{bh} - p), \tag{4.7}$$

where $p = p_0$ and the equivalent radius r_e equals

$$r_e = \exp\left(\left[\sum_i T_{0i} \ln r_i - 2\pi \right] / \sum_i T_{0i} \right). \tag{4.8}$$

We consider an example where the support of φ_0 is shown as in Fig. 4.3 and the medium is isotropic. In this case,

$$T_{01} = T_{02} = T_{04} = T_{05} = 1, \quad T_{03} = T_{06} = 0, \tag{4.9}$$

and

$$r_e = he^{-\pi/2} = 0.20788\ldots, \tag{4.10}$$

which is exactly the same as that in the finite difference method. This is not surprising because the finite element method is a five-point stencil scheme for the case shown in Fig. 4.3 [4, 5].

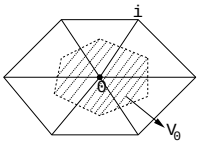

Fig. 5.1. V_0 for the linear finite element.

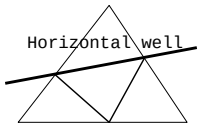

Fig. 5.2. A horizontal well through two edges.

4.2. Rectangular finite elements. Again, for brevity of presentation, we consider the simplest rectangular finite element, the bilinear finite element [4]. As an example, let the support of φ_0 be given as in Fig. 4.4. In this case, equation (4.1) remains valid. Because of the symmetry assumption of radial flow, $p_1 = p_3 = p_5 = p_7$ and $p_2 = p_4 = p_6 = p_8$. Consequently, from (4.1) with Ω_0 as in Fig. 4.4, simple algebraic computations imply

$$\frac{4}{3}\frac{\rho\sqrt{k_{11}k_{22}}h_3}{\mu}(2p_0 - p_1 - p_2) = q. \tag{4.11}$$

Using the analytic model (2.5), we see that

$$\begin{aligned} p_1 &= p_{bh} - \frac{\mu q}{2\pi\rho\sqrt{k_{11}k_{22}}h_3}\ln\left(\frac{h}{r_w}\right), \\ p_2 &= p_{bh} - \frac{\mu q}{2\pi\rho\sqrt{k_{11}k_{22}}h_3}\ln\left(\frac{\sqrt{2}h}{r_w}\right). \end{aligned} \tag{4.12}$$

Combining equations (4.11) and (4.12) yields the well model (4.7) with the equivalent radius

$$r_e = 2^{1/4}e^{-3\pi/4}h. \tag{4.13}$$

5. Control Volume Finite Element Methods

The finite difference method presented in the third section is locally conservative, but is not flexible in the treatment of complex reservoirs. On the other hand, the standard finite element method described in the fourth section is more flexible, but not conservative on local elements (e.g., on triangles). It is globally conservative. In this section, we consider a variation of the finite element method so that it is locally conservative on each control volume. Control volumes can be formed around grid nodes by joining the midpoints of the edges of a triangle with a point inside the triangle, for example (Fig. 5.1). Different locations of the point give rise to different forms of the flow term between grid nodes. When it is the barycenter of the triangle, the resulting grid is of CVFE (control volume finite element) type, and the resulting finite element method is the CVFE method. This method was first introduced by Lemonnier [14] for reservoir simulation. The CVFE grids are different from the PEBI (perpendicular bisection) grids (also called Voronoi grids [12]) in that the latter are locally orthogonal. The CVFE grids are more flexible.

5.1. Well model equations. For the CVFE method based on the triangular linear elements [5], the well model equation (4.7) and the equivalent radius r_e defined in (4.8) remain the same since the linear system arising from this method is the same as that from the standard finite element method using piecewise linear functions [5]. For the CVFE, node $\mathbf{x}_0$ is now the center of a control volume; i.e., the well is now located at a center (Fig. 5.1), instead of at a vertex as in the standard

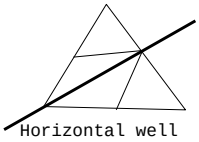

Fig. 5.3. A horizontal well through a vertex.

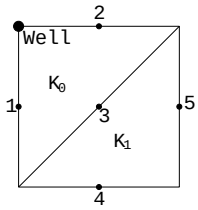

Fig. 6.1. Well location for triangular mixed elements.

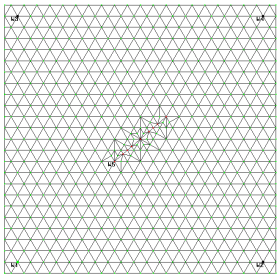

Fig. 5.4. A horizontal well for the triangular case.

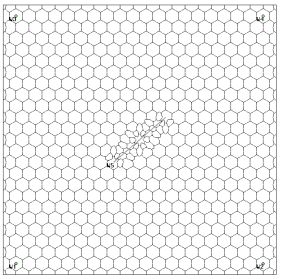

Fig. 5.5. A horizontal well for the CVFE case.

finite element method. In practice, the equivalent radius r_e for the CVFE can be approximated using a simpler formula:

$$r_e = \sqrt{\frac{|V_0|}{\pi}}, \tag{5.1}$$

where $|V_0|$ is the area of the control volume V_0 that contains the well (Fig. 5.1). The derivation of (5.1) is based on the following principle: $|V_0|$ is approximately the area of a circle with radius r_e that contains the well and the mean value of pressure on V_0 is approximately the pressure on this circle. The extension to the CVFE based on the rectangular bilinear elements can be similarly carried out.

5.2. Horizontal wells. The well model derived for a vertical well using finite elements can be generalized to include the following effects: gravity forces, anisotropic reservoirs, skin factors, horizontal wells, and multiphase flows. These generalizations can be performed in the same fashion as in the finite difference case; here we focus on the modeling of horizontal wells in arbitrary directions which cannot be easily done using finite differences. The medium is assumed to be isotropic.

Due to the intrinsic flexibility of finite element grids, the flow pattern near a horizontal well in an arbitrary direction can be modeled accurately, particularly when local grid refinement is used. If the horizontal well passes through a triangle, this triangle needs be refined: (1) If it passes through two edges of the triangle, we can make the intersections to be the vertices of smaller triangles (or centers of control volumes) by properly adjusting the midpoints of the two edges (Fig. 5.2); (2) If it passes through a vertex of the triangle, the local refinement can be done as in Fig. 5.3 by connecting the well-edge intersection with the two midpoints of the other edges. The feature of this approach is that the horizontal well contains only triangle vertices (Fig. 5.4) or control volume centers (Fig. 5.5).

For the CVFE, the well model equation for a horizontal well in an arbitrary direction is derived in an analogous fashion to (4.7):

$$q = \frac{2\pi\rho k\Delta L}{\mu \ln(r_e/r_w)}(p_{bh} - p), \tag{5.2}$$

where ΔL is the diameter of the control volume (that contains the well) in the well direction and the equivalent radius r_e can be defined as in (4.8). For the latter, using a similar approximation principle as for (5.1), a simpler definition is

$$r_e = \sqrt{\frac{|V_0|h_3}{\pi \Delta L}}, \tag{5.3}$$

where h_3 is the x_3-spatial grid size of the block that contains the well. An extension of (5.2) to multiphase flow can be given:

$$q_\alpha = \frac{2\pi k \Delta L}{\ln(r_e/r_w) + s_k} \frac{\rho_\alpha k_{r\alpha}}{\mu_\alpha} \left(p_{bh} - p_\alpha - \rho_\alpha \wp(z_{bh} - z)\right).$$

6. Mixed Finite Element Methods

The primary reason for using mixed finite element methods is that in some applications a vector variable (e.g., a fluid velocity) is the main variable in which one is interested. Then the mixed methods are developed to approximate both this variable and a scalar variable (e.g., pressure) simultaneously and to give a high order approximation of both variables. Mixed finite element methods use two approximation spaces, $\mathbf{V}_h$ for velocity and W_h for pressure [4]. In the case of a no-flow boundary condition on the external boundary Γ of $\Omega \subset \mathbb{R}^2$, for example, the mixed weak formulation of equations (2.1) and (2.2) is

$$\begin{aligned} &\mu \int_\Omega \mathbf{k}^{-1}\mathbf{u} \cdot \mathbf{v}\ d\mathbf{x} - \int_\Omega \nabla \cdot \mathbf{v} p\ d\mathbf{x} = 0 \qquad && \forall \mathbf{v} \in \mathbf{V}_h, \\ &\rho h_3 \int_\Omega \nabla \cdot \mathbf{u} w\ d\mathbf{x} = q w(\mathbf{x}_0) && \forall w \in W_h, \end{aligned} \tag{6.1}$$

where $\mathbf{x}_0$ is the well location and $\mathbf{V}_h \subset \mathbf{V}$, with $\mathbf{V}$ given by [4]

$$\mathbf{V} = \{\mathbf{v} = (v_1, v_2) \in \mathbf{H}(\mathrm{div}, \Omega) :\ \mathbf{v} \cdot \boldsymbol{\nu} = 0 \text{ on } \Gamma\}.$$

In this section, we consider the lowest-order Raviart-Thomas mixed spaces on rectangles and triangles [20]. As an example, we consider an isotropic medium.

6.1. Rectangular mixed spaces. Let K_h be a partition of a rectangular domain Ω into rectangles such that the horizontal and vertical edges of rectangles are parallel to the x_1- and x_2-coordinate axes, respectively, and adjacent elements completely share their common edge. The spaces $\mathbf{V}_h$ and W_h are

$$\begin{aligned} \mathbf{V}_h = \{&\mathbf{v} \in \mathbf{V} :\ \mathbf{v}\big|_K = (b_K x_1 + a_K, d_K x_2 + c_K), \\ &a_K, b_K, c_K, d_K \in \mathbb{R},\ K \in K_h\}, \\ W_h = \{&w :\ w \text{ is constant on each rectangle in } K_h\}. \end{aligned}$$

As an example, we consider the case where $\mathbf{x}_0$ is located in the center of a rectangle (Fig. 3.1). In this case, the mixed method (6.1) reduces to a five-point stencil scheme as in (3.1) [21], and the well model equation (3.4) and its extensions derived in Section 3.2 remain exactly the same.

6.2. Triangular mixed spaces. Let K_h be a triangulation of a polygonal domain Ω into triangles such that no vertex of one triangle lies in the interior of an edge of another triangle. In the triangular case, the spaces $\mathbf{V}_h$ and W_h are

$$\begin{aligned} \mathbf{V}_h = \{&\mathbf{v} \in \mathbf{V} :\ \mathbf{v}\big|_K = (b_K x_1 + a_K, b_K x_2 + c_K), \\ &a_K, b_K, c_K \in \mathbb{R},\ K \in K_h\}, \\ W_h = \{&w :\ w \text{ is constant on each triangle in } K_h\}. \end{aligned}$$

As an example, we consider the quarter plane symmetry case where the well is located at the corner $\mathbf{x}_0$ of a square that is subdivided into two triangles by connecting the vertices adjacent to the well vertex (Fig. 6.1). The pressure and velocity nodes are indicated as in Fig. 6.1.

Let $\boldsymbol{\varphi}_i$ be the velocity basis functions corresponding to the nodes $\mathbf{x}_i$ ($i = 1, 2, 3, 4, 5$). Set

$$\mathbf{u} = \sum_{i=1}^{5} u_i \boldsymbol{\varphi}_i,$$

where u_i denotes the normal component of $\mathbf{u}$ at $\mathbf{x}_i$. Via symmetry, the correct boundary condition is no-flow on the x_1 and x_2 boundary edges, which implies that $u_1 = u_2 = 0$.

It can be seen that

$$\boldsymbol{\varphi}_3 = \begin{cases} \dfrac{\sqrt{2}}{h}(x_1, x_2), & (x_1, x_2) \in K_0, \\ \dfrac{\sqrt{2}}{h}(h - x_1, h - x_2), & (x_1, x_2) \in K_1, \end{cases} \tag{6.2}$$

where h is the grid size in the x_1 and x_2 directions. It can be also checked that

$$\int_\Omega \boldsymbol{\varphi}_3 \cdot \boldsymbol{\varphi}_4 \, d\mathbf{x} = \int_\Omega \boldsymbol{\varphi}_3 \cdot \boldsymbol{\varphi}_5 \, d\mathbf{x} = 0. \tag{6.3}$$

Taking $\mathbf{v} = \boldsymbol{\varphi}_3$ in the first equation of (6.1) and using (6.3) gives

$$u_3 \int_{K_0 \cup K_1} \boldsymbol{\varphi}_3 \cdot \boldsymbol{\varphi}_3 \, d\mathbf{x} - \frac{k}{\mu} \int_{K_0 \cup K_1} \nabla \cdot \boldsymbol{\varphi}_3 p \, d\mathbf{x} = 0,$$

so

$$u_3 \frac{2h^2}{3} - \frac{k}{\mu}(p_0 - p_1)\sqrt{2}h = 0, \tag{6.4}$$

where p_0 and p_1 are the pressure values on K_0 and K_1, respectively.

Next, by quarter plane symmetry and using (6.2), choosing $w = 1$ on K_0 and $w = 0$ elsewhere in the second equation of (6.1) yields

$$4\sqrt{2}\rho h_3 u_3 h = q. \tag{6.5}$$

Combining equations (6.4) and (6.5) implies

$$p_0 - p_1 = \frac{q\mu}{12\rho k h_3}. \tag{6.6}$$

For the value p_1, we use the well equation (2.5):

$$p_1 = p_{bh} - \frac{\mu q}{2\pi\rho k h_3} \ln\left(\frac{r_1}{r_w}\right), \tag{6.7}$$

where $r_1 = 2\sqrt{2}h/3$ is the distance from the well to the barycenter of the triangle K_1. Substituting (6.7) into (6.6) generates the well model equation (3.4) with the equivalent radius

$$r_e = \frac{2\sqrt{2}h}{3} e^{-\pi/6}. \tag{6.8}$$

7. Numerical Experiments

The example simulates a transient problem with an imposed well flow rate, and the wellbore pressure and the field pressure in the vicinity of the well have analytical solutions [5]. An isolated well is located in the center of a large domain with a size of 13,500 ft in the x_1- and x_2-directions. The rock and fluid properties are given in Table 7.1.

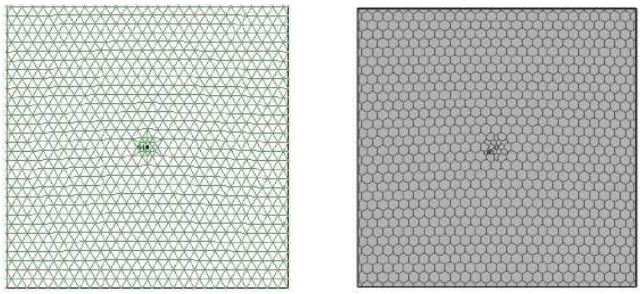

Fig. 7.1. Base triangles and control volumes.

The standard finite element method on triangles and control volume finite element method are used in the numerical well modeling (see Sections 4.1 and 5.1). In these two cases, the well model is given by (4.7). A local refinement with a refined area of 19,627.7 ft^2 is employed; see Fig. 7.1, where a two-level refinement is shown. One of the advantages using triangular elements is that local uniform grids in the vicinity of the well can be used. The comparisons between the numerical pressure p_h and the analytical pressure p at $r = r_w$ are shown in Table 7.2 from which we see that the absolute error on the pressure computation is less than 0.01, which shows the accuracy of the numerical model.

Table 7.1. Parameters for a reservoir

Item	Description	Unit	Value
q	Oil production rate	STB/D	300
μ	Oil viscosity	cp	1.06
k	Permeability	md	300
h_3	Thickness	ft	100
c_o	Oil compressibility (i.e., c_f)	1/psi	0.00001
c_R	Rock compressibility	1/psi	0.000004
ϕ	Porosity	fraction	0.2
p_0	Initial pressure	psia	3,600
r_w	Radius of wellbore	ft	0.1875
x_{1max}	Length in the x_1-direction	ft	13,500
x_{2max}	Length in the x_2-direction	ft	13,500
h	Length of triangles used in simulation	ft	300
A	Local refinement area near wellbore	ft^2	19,627.7

Table 7.2. The pressure comparison at $r = r_w$.

Time	Time	$r^2/(4t\chi)$	p_h	p	$p_h - p$
days	sec	$\times 10^{-8}$	psia	psia	psia
0.1	8,640	13.740	3,596.32	3,596.32	0.00
0.2	17,280	6.870	3,595.47	3,595.46	0.01
0.3	25,920	4.580	3,595.07	3,595.06	0.01
0.4	34,560	3.435	3,594.80	3,594.80	0.00
0.5	43,200	2.748	3,594.60	3,594.60	0.00
0.6	51,840	2.290	3,594.45	3,594.44	0.01
0.7	60,480	1.963	3,594.31	3,594.31	0.00
0.8	69,120	1.718	3,594.20	3,594.19	0.01
0.9	77,760	1.527	3,594.10	3,594.09	0.01
1.0	86,400	1.374	3,594.01	3,594.01	0.00
1.5	129,600	0.916	3,593.69	3,593.68	0.01
2.0	172,800	0.687	3,593.46	3,593.45	0.01
2.5	216,000	0.550	3,593.28	3,593.27	0.01
3.0	259,200	0.458	3,593.13	3,593.12	0.01
4.0	345,600	0.344	3,592.90	3,593.90	0.00

References

[1] J. E. Aarnes, On the use of a mixed multiscale finite element method for greater flexibility and increased speed or improved accuracy in reservoir simulation, *Multiscale Model. Simul.* **2** (2004), 421–439.

[2] D. K. Babu, A. S. Odeh, A.-J. Al-Khalifa and R. C. McCann, The relation between wellblock and well pressure in numerical simulation of horizontal wells-general formulas for arbitrary well locations in grids, SPE Paper 20161, June 1989.

[3] J. Bear, Dynamics of Fluids in Porous Media, Dover, New York, 1972.

[4] Z. Chen, Finite Element Methods and Their Applications, Springer-Verlag, Heidelberg and New York, 2005.

[5] Z. Chen, G. Huan and Y. Ma, Computational Methods for Multiphase Flows in Porous Media, in the Computational Science and Engineering Series, Vol. 2, SIAM, Philadephia, PA, 2006.

[6] Z. Chen and X. Y. Yue, Numerical homogenization of well singularities in the flow transport through heterogeneous porous media, *Multiscale Modeling and Simulation* **1** (2003), 260–303.

[7] P. G. Ciarlet, The Finite Element Method for Elliptic Problems, North-Holland, Amsterdam, 1978.

[8] Y. Ding, A generalized 3D well model for reservoir simulation, *SPE J.* (1996), 437–450.

[9] Y. Ding and L. Jeannin, New numerical schemes for near-well modelling using flexible grids, *SPE J.* (March) (2004), 109–121.

[10] R. E. Ewing, R. D. Lazarov, S. L. Lyons, D. V. Papavassiliou, J. E. Pasciak and G. Qin, Numerical well model for non-Darcy flow through isotropic porous media, *Computational Geosciences* **3** (1999), 185–204.

[11] V. A. Garanzha, V. N. Konshin, S. L. Lyons, D. V. Papavassilion, and G. Qin, Validation of non-Darcy well models using direct numerical simulation, In Numerical Treatment of Multiphase Flows in Porous Media, Proceedings of the International Workshop Held in Beijing, China, Lecture Notes in Physics, Vol 552, Z. Chen et al. (Eds.), Springer-Verlag, Heidelberg, 1999, 156–169.

[12] B. Heinrich, Finite Difference Methods on Irregular Networks, Birkhauser, Basel, Boston, Stuttgart, 1987.

[13] S. H. Lee and W. J. Milliken, The productivity index of an inclined well in finite-difference reservoir simulation, SPE Paper 25247, 12th SPE Symposium on Reservoir Simulation, New Orleans, LA, 1993, 143–153.

[14] P. A. Lemonnier, Improvement of reservoir simulation by a triangular discontinuous finite element method, SPE paper 8249 presented at the 1979 Annual Fall Technical Conference and Exhibition of SPE of AIME, Las Vegas, Sept. 23–26, 1979.

[15] L. S. Nghiem, D. A. Collins and R. Sharma, Seventh SPE comparative solution project: Modeling of horizontal wells in reservoir simulation, SPE 21221, 11th SPE Symposium on Reservoir Simulation in Anaheim, California, Feb. 17-20, 1991.

[16] C. L. Palagi and K. Aziz, Handling wells in simulators, *Proc. Fourth Intl. Forum on Reservoir Simulation*, Salzburg, Austria, 1992.
[17] D. W. Peaceman, Interpretation of well-block pressures in numerical reservoir simulation, SPE 6893, 52nd Annual Fall Technical Conference and Exhibition, Denver, 1977.
[18] D. W. Peaceman, Interpretation of well-block pressures in numerical reservoir simulation with non-square grid blocks and anisotropic permeability, *Soc. Pet. Eng. J.*, June (1983), 531–543.
[19] D. W. Peaceman, Presentation of a horizontal well in numerical reservoir simulation, SPE 21217, presented at 11th SPE Symposium on Reservoir Simulation in Ananheim, California, Feb. 17-20, 1991.
[20] R. Raviart and J.-M. Thomas, A mixed finite element method for second order elliptic problems, Lecture Notes in Mathematics, vol. 606, Springer, Berlin, 292–315, 1977.
[21] T. F. Russell and M. F. Wheeler, Finite element and finite difference methods for continuous flows in porous media, the Mathematics of Reservoir Simulation, R. E. Ewing, ed., SIAM, Philadelphia, 35–106, 1983.
[22] C. Wolfsteiner, L. J. Durlofsky, and K. Aziz, Calculation of well index for nonconventional wells on arbitrary grids, *Computational Geosciences* **7** (2003), 61–82.

Department of Chemical and Petroleum Engineering, Schulich School of Engineering, University of Calgary, 2500 University Drive N.W. Calgary, Alberta T2N 1N4, Canada and Faculty of Science, Xi'an Jiaotong University, Xi'an 710049, P. R. China
E-mail: zhachen@ucalgary.ca

Department of Mathematics, Box 750156, Southern Methodist University, Dallas, TX 75275-0156, USA
E-mail: yzhang@smu.edu